

In Situ X-ray Study of the Solid Electrolyte Interphase (SEI) Formation on Graphene as a Model Li-ion Battery Anode

Sudeshna Chattopadhyay,^{§,†} Albert L. Lipson,^{§,†} Hunter J. Karmel,[†] Jonathan D. Emery,[†] Timothy T. Fister,[‡] Paul A. Fenter,[‡] Mark C. Hersam,^{*,†} and Michael J. Bedzyk^{*,†}

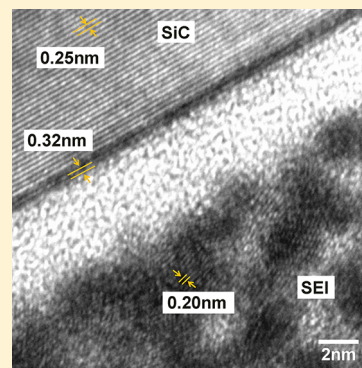
[†]Department of Materials Science and Engineering, Northwestern University, Evanston, Illinois 60208, United States

[‡]Chemical Sciences and Engineering Division, Argonne National Laboratory, Lemont, Illinois 60439, United States

S Supporting Information

ABSTRACT: The solid electrolyte interphase (SEI) plays a critical role in the performance and safety of Li-ion batteries, but the crystal structure of the materials formed have not been previously studied. We employ the model system of epitaxial graphene on SiC to provide a well-defined graphitic surface to study the crystallinity and texture formation in the SEI. We observe, via in situ synchrotron X-ray scattering, the formation and growth of LiF crystallites at the graphene surface, which increase in size with lithiation dose and are textured such that the LiF (002) planes are approximately parallel to the graphene sheets. Furthermore, X-ray photoelectron spectroscopy (XPS) reveals the composition of the SEI formed in this system to consist of LiF and organic compounds similar to those found previously on graphite. SEI components, other than LiF, do not produce X-ray diffraction peaks and are categorized as amorphous. From high-resolution transmission electron microscopy, the LiF crystallites are seen in near proximity to the graphene surface along with additional apparently amorphous material, which is likely to be other SEI components detected by XPS and/or misoriented LiF. This new understanding that LiF crystallites grow on the graphene surface with strong texturing will assist future efforts to model and engineer the SEI formed on graphitic materials.

KEYWORDS: Li-ion batteries, solid electrolyte interphase, graphene, graphite, X-ray scattering



INTRODUCTION

The performance, lifetime, and safety of batteries need to be enhanced to enable emerging areas of technology, such as electric vehicles. During cycling, a layer of decomposed electrolyte, known as the solid electrolyte interphase (SEI), forms on Li-ion battery electrodes.¹ Since the SEI is formed from the breakdown of the electrolyte, it reduces the capacity of the battery and can be detrimental to cell lifetime. On the other hand, the stability and passivating qualities of the SEI are important to limit uncontrolled reactions, which can pose safety risks resulting from catastrophic failure.²

The SEI previously has been studied using a variety of in situ methods including atomic force microscopy (AFM), scanning ion conductance microscopy (SICM), Fourier-transform infrared (FTIR) spectroscopy, and ellipsometry.^{3–7} Ex situ studies, using X-ray photoelectron spectroscopy (XPS) and scanning electron microscopy (SEM), have been utilized to probe the SEI composition and morphology.^{8–10} These studies show that SEI formation on the anode surface is more pronounced than that on the cathode,¹¹ and its composition depends on the choice of electrolyte and electrode materials.^{11,12} Although the SEI is critical to the operation of Li-ion batteries, its structure and evolution are not fully understood.

The most commonly used anode material in commercial Li-ion batteries is graphitic carbon. The composition of the SEI on

graphite with fluorinated electrolytes has been found to include hydrocarbons, lithium alkyl carbonates, LiOH, Li₂CO₃, Li₂O, and LiF.^{7,8,10,13–16} LiF was shown to grow in the SEI, but no structural study (to our knowledge) was previously performed.¹⁰ Consequently, the structural relationships (if any) between the LiF and the electrode surface are not well-established. LiF is postulated to form from decomposition/reduction of the LiPF₆ salt (due to its thermal and chemical instabilities), via the reaction $\text{LiPF}_6 \leftrightarrow \text{Li}^+\text{F}^- \downarrow + \text{PF}_5$ and many other possible reactions.^{12,15,17,18} Furthermore, the SEI was found to grow thicker and with different composition on the edge planes of graphite as compared to the basal plane.^{8,19–21} To reduce the total irreversible capacity of the system, while still allowing fast Li⁺ diffusion into the anode via the edge surfaces, a combination of basal and edge surfaces is used. An understanding of the SEI on both the basal and edge planes of graphite is therefore necessary in order to understand how to optimize anode morphology.

X-ray scattering can probe interfacial systems in situ, is nondestructive, and can determine the interfacial structure at the atomic scale. In situ and ex situ X-ray diffraction have

Received: May 23, 2012

Revised: July 10, 2012

Published: July 23, 2012



previously been used to study the bulk crystal structure of Li-ion battery electrodes during cycling,^{22–30} but it has not yet been utilized to study the structure of the SEI. Consequently, there is little information about the crystallinity and morphology of the SEI.

We have employed a model system of epitaxial graphene on 6H-SiC (EG/SiC) for these studies. Graphene sheets provide a well-defined graphitic surface that is not perturbed during lithiation.³¹ These graphene sheets fully cover the SiC with domains of ~ 200 nm and therefore possess a high percentage of basal plane area and minimal edge plane sites. Consequently, this system provides a model substrate for probing SEI formation on graphitic basal planes. Furthermore, in this system, the graphene sheets are exceptionally parallel to the SiC (0006) basal planes³¹ enabling the study of texture formation (i.e., preferential orientation of crystals) in the SEI that is not possible with graphitic substrates having substantial mosaic disorder and surface roughness. Preferential orientation of crystallites in the SEI may modify the rate of Li^+ diffusion to the electrode surface through those crystals, which could change the rate performance of the battery.^{32,33}

Herein, we report our studies on the atomic structure of the SEI formed on EG/SiC. XPS studies show SEI components on EG/SiC that are similar to that found previously on graphite anodes. Furthermore, we find that LiF crystallites form and grow on the EG/SiC surface with strong texturing during lithiation via in situ synchrotron X-ray scattering. Lastly, using high-resolution transmission electron microscopy (HRTEM), we observe the structure and morphology of the SEI on the EG/SiC surface.

EXPERIMENTAL SECTION

SiC samples were n-type doped single crystal wafers purchased from CREE. As described elsewhere,³¹ the SiC(0001) substrates were cleaned with acetone and isopropanol before being graphitized in ultrahigh vacuum. Scanning tunneling microscopy (STM) revealed that the surfaces were covered by a combination of single and bilayer graphene with minimal $6\sqrt{3} \times 6\sqrt{3}$ reconstruction exposed. The electrolyte was 1 M LiPF_6 (99.99%, Sigma-Aldrich) in 1:1 ethylene carbonate (EC) to dimethyl carbonate (DMC) (anhydrous, Sigma-Aldrich), and the counter electrode was metallic Li (Sigma-Aldrich). The samples for the XPS and HRTEM measurements were lithiated galvanostatically in a two electrode beaker type cell with a current of $21 \mu\text{A}/\text{cm}^2$. The sample used for the X-ray scattering experiment was lithiated in a home-built in situ X-ray thin-film³⁴ cell with a $7.5 \mu\text{m}$ Kapton window (see Supporting Information, S1). The cell was sealed in an inert atmosphere using a combination of Kapton film, a Viton gasket, and pipe fittings. The seal was leak tested, and the Li metal counter electrode showed no significant oxidation when examined after the X-ray experiments, which is consistent with an insignificant amount of water inside the cell. The galvanostatic lithiation of this sample started at a current of $0.032 \text{ mA}/\text{cm}^2$ until a charge of $0.13 \text{ mAh}/\text{cm}^2$, then $0.064 \text{ mA}/\text{cm}^2$ until $0.26 \text{ mAh}/\text{cm}^2$, and last $0.13 \text{ mA}/\text{cm}^2$ until $0.51 \text{ mAh}/\text{cm}^2$.

XPS measurements were taken using an ESCA Probe (Omicron) after samples were cleaned with isopropanol to remove residual electrolyte. The spectra were smoothed by using fast Fourier transform (FFT) filtering to remove noise. A peak fitting procedure was used to find the exact peak positions listed in Table 1.

X-ray scattering experiments were performed at sector SID-C (DND-CAT) at the Advanced Photon Source using 17.00 keV photons in a reflection geometry (see Supporting Information, S2). Two detectors were used during these experiments: a charge coupled device (CCD) area detector (“Roper CCD”) (Princeton Instruments 7501-0002) mounted on the detector arm of the diffractometer³⁵ and a MAR165 large area CCD detector (“MAR CCD”) (MAR Research)

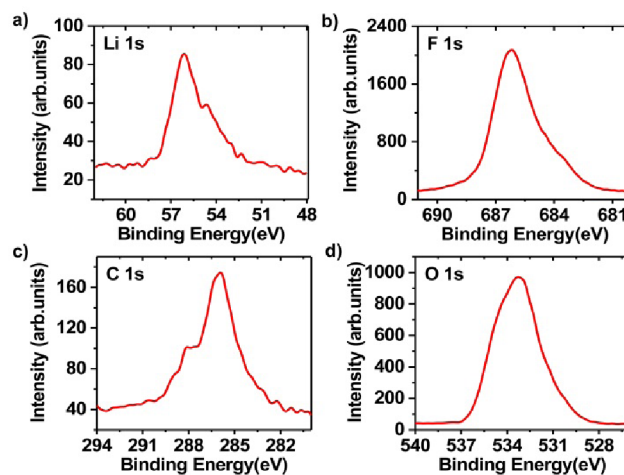


Figure 1. Ex situ XPS spectra for a $14 \text{ mAh}/\text{cm}^2$ lithiated EG/SiC sample using 1 M LiPF_6 in 1:1 EC/DMC electrolyte for (a) Li 1s, (b) F 1s, (c) C 1s, and (d) O 1s.

centered on the beam path after the sample. The diffraction data from the SEI (i.e., intensity vs momentum transfer, q_z , measured near the surface normal direction) was extracted from the Roper CCD images by masking-out the true specularly reflected X-ray beam from the images, integrating the image along q_x , and plotting the remaining near-specular scattering intensity vs q_z . Using Nika software, the MAR CCD images were converted into reciprocal space maps and ‘pole figures’ were extracted.³⁶ For the LiF (002) pole figure, a combination of MAR CCD images were taken at incident angles of 5° and 10.384° . 10.384° is the local specular position for LiF (002), meaning that LiF crystals with their (002) planes parallel to the SiC (0006) planes satisfy the Bragg condition at this incident angle. The pole figure for LiF (111) was extracted from those same two images and an image near to the local specular from the Roper CCD (see Supporting Information, S3). The extracted data for both LiF (002) and (111) were merged, as was proposed by Baker et al. to remove artifacts created by the geometry.³⁷

The sample for HRTEM was prepared using focused ion beam milling procedures, as described previously.³¹ HRTEM was performed using a JEM-2100F TEM (JEOL) at 200 kV .

RESULTS AND DISCUSSION

Ex situ XPS was utilized to investigate the surface composition of the SEI formed on EG/SiC. The resulting spectra for a $14 \text{ mAh}/\text{cm}^2$ lithiated EG/SiC sample using 1 M LiPF_6 in 1:1 EC/DMC electrolyte are shown in Figure 1, and peak positions with proposed assignments are given in Table 1. The Li 1s

Table 1. Binding Energies and Proposed Assignments for the XPS Spectra for a $14 \text{ mAh}/\text{cm}^2$ Lithiated EG/SiC Sample Using 1 M LiPF_6 in 1:1 EC/DMC Electrolyte

element	binding energy (eV)	proposed assignment	ref
Li	56.1	LiF	8, 10, 15, 16
Li	54.7	Li–O (R-CH ₂ OCO ₂ Li, LiOH and Li-O-graphite) or polymer	8, 15
F	686.2	LiF	8, 10
C	286	Polymer (PEO)	10
C	288.1	R-CH ₂ OCO ₂ Li	10
C	289	R-CH ₂ OCO ₂ Li	10
O	533.4	C–O bonds	8, 10
P	135	unassigned	15

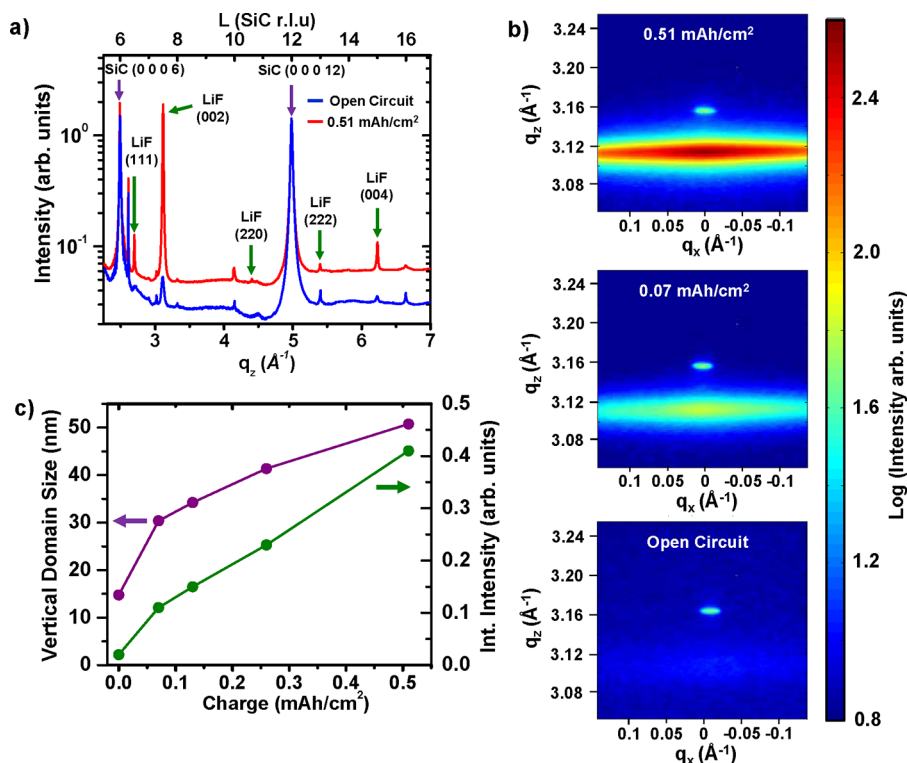


Figure 2. X-ray scattering data from an in situ lithiated EG/SiC sample. (a) Diffraction pattern extracted from the images taken using the Roper CCD camera in the specular geometry for the sample at open circuit and at 0.51 mAh/cm² lithiation. (b) CCD images around the LiF (002) Bragg peak (incidence angle of 10.609°) at different lithiation stages. The LiF (002) Bragg peak is observed at $q_z = 3.11 \text{ \AA}^{-1}$, while the small central spot in each image (at $q_z = 3.16 \text{ \AA}^{-1}$) corresponds to the scattering intensity from the surface rod of EG/SiC interface. (c) Domain size and integrated intensity of the LiF (002) Bragg peak in the window of the Roper CCD at different lithiation states.

spectrum shows a strong peak at a binding energy of 56.1 eV indicating the formation of LiF.^{8,10,15,16} There is also a peak at 54.7 eV corresponding possibly to Li–O bonds (e.g., R-CH₂OCO₂Li, LiOH, and Li–O-graphite) or a lithium containing polymer.^{8,15} In Figure 1b, the F 1s spectrum shows a peak at 686.2 eV, further indicating LiF.^{8,10} Note that there is no peak at 688 eV, which would indicate residual LiPF₆.^{10,16} In the C 1s spectra, there are three peaks at 286 eV, 288.1 eV, and 289 eV. The peak at 286 eV could be a polymer such as polyethylene oxide (PEO) with C–O bonds, which can be formed via the polymerization of EC.¹⁰ The other two peaks can be assigned to the two carbons in R-CH₂OCO₂Li.¹⁰ There is no evidence for Li₂CO₃, which has a peak between 290.5 and 291.5 eV. The O 1s spectrum is shown in Figure 1d with a strong peak at 533.4 eV, which is consistent with a variety of C–O bonds.^{8,10} There is also a peak from the P 2p at 135 eV, which is not LiPF₆ and cannot be assigned.¹⁵ These SEI compounds are consistent with those found previously on graphite with similar electrolytes.^{8,10,15,16}

To understand the atomic structure of the SEI components during growth, we utilized in situ synchrotron X-ray scattering. Figure 2 shows the scattering data taken using the Roper CCD near the specular reflection condition for the SiC. The diffraction pattern (Figure 2a) shows four peaks between 2.2 \AA^{-1} and 7 \AA^{-1} that increase in intensity after lithiation (0.51 mAh/cm²). These peaks correspond to the (111), (002), (220), and (004)³⁸ for cubic LiF in the rock salt structure, as indicated in Figure 2a. There appears to be nonzero intensity at the peak location for LiF (222) at open circuit due to interference from the SiC (0 0 0 13) quasi-Bragg peak. There is, however, a trace of LiF present at open circuit voltage as can be

seen by the nonzero (002) and (004) peaks (this intensity corresponds to <5% of the total LiF that was observed at 0.51 mAh/cm² lithiation). The strong peaks at about $q_z = 2.5 \text{ \AA}^{-1}$ and 5 \AA^{-1} and the weaker peaks near $q_z = 4.1 \text{ \AA}^{-1}$ and 6.6 \AA^{-1} correspond to diffuse scattering originating from the SiC (0 0 0 6), (0 0 0 12), (0 0 0 10), and (0 0 0 16) Bragg and quasi-Bragg peaks, respectively (the data at and very near the SiC Bragg peaks have been excluded in this plot). There is no additional scattering intensity from other potential SEI components, all of which would be expected to diffract in this q -range; therefore, we conclude that LiF is the only crystalline component in the SEI.

Figure 2b shows the scattering pattern near the LiF (002) Bragg peak at different lithiation stages, where the small oval spot is the true specular surface reflection, and the broader line of intensity derives from the (002) LiF Bragg peak. It should be noted that due to the $>2^\circ$ LiF mosaic width the intensity and peak shape for LiF (002) do not change appreciably between this position and the local specular position, where the peak aligns with the surface reflection. These scattering patterns show that the intensity of this peak increases with lithiation, but without any significant change in the mosaic width. Furthermore, the central spot in the images, corresponding to the surface specular reflection of EG/SiC, is unchanged at different lithiation stages (in either intensity or shape), indicating that the graphene structure is not disturbed.³¹ Figure 2c shows the evolution of the LiF (002) Bragg peak integrated intensity and vertical domain size at various lithiation states. The average crystal size (measured along the surface normal direction) increases monotonically with increasing lithiation and reaches a value of $\sim 50 \text{ nm}$ at 0.51 mAh/cm². The

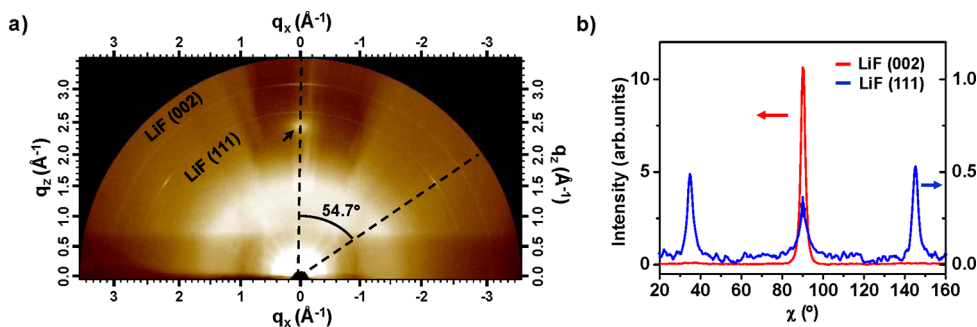


Figure 3. (a) In situ diffraction pattern of 0.51 mAh/cm² lithiated EG/SiC taken with the MAR CCD at an incidence angle of 5°. The arrow in the image indicates the diffuse SiC (0006) peak. (b) Extracted pole figure for the image shown in part a and images at the specular positions for the LiF (111) (right y-axis) and (002) peaks (left y-axis), with background subtraction and polarization correction, stitched near to 90° in χ .

integrated intensity of the LiF (002) in the window of the Roper CCD increases nearly linearly with charge.

These data also reveal information concerning the orientation of the LiF crystals. The intensity of the LiF (002) peak is more than an order of magnitude larger than that of the LiF (111) peak, indicating a preferential orientation of the LiF (002) planes approximately parallel to the SiC (0006) planes. Since the intensity ratio calculated for a LiF powder is 4:3,³⁹ this suggests that a large fraction of the LiF has the (002) orientation. While the LiF (002) peak is most intense along the specular direction (here, indicated as $q_x = 0 \text{ \AA}^{-1}$), we do not see any contribution from the LiF (002) Bragg peak to the surface reflectivity, suggesting that while the LiF is preferentially aligned, it is not epitaxial with the graphene.

We have also employed a large area detector to collect the powder rings of LiF (002) and LiF (111) to probe the full LiF texture.^{37,40–42} Figure 3a shows the diffraction pattern of EG/SiC lithiated to 0.51 mAh/cm² taken using the MAR CCD at an incidence angle of 5°. At q below 2.3 \AA^{-1} , there is additional diffraction intensity from the Kapton window³⁴ and the electrolyte (note that the sample holder clips this image for $q_z < 0.7 \text{ \AA}^{-1}$ causing the shadow).

Figure 3b shows the complete pole figures (between 20° and 160° in χ , see Supporting Information, S2 for geometry) for the LiF (111) and (002) peaks. The pole figure is extracted by merging both the diffraction pattern at an incidence angle of 5° and the local specular positions (shown in Supporting Information, Figure S3), including background subtraction and correction for the horizontally polarized X-ray beam.³⁷ Since the SEI layer is more than 100 nm thick,³¹ an incidence angle of 5° was chosen instead of grazing incidence to reduce the effects of absorption and beam footprint, which would change the probed region for the two measurements.³⁷ The LiF (002) peak is strongest at $\chi = 90^\circ$, while the LiF (111) is most intense at 35° and 145°. These peaks are due to strong texturing with crystals oriented such that the LiF (002) planes are parallel to the graphene sheets. The full width at half-maximum of the LiF (002) peak at $\chi = 90^\circ$ is approximately 2.4°, indicating a narrow mosaic distribution of LiF orientations in the SEI. It should be noted that the signal from the surface rod at this momentum transfer (q_z) contributes less than 1% to the integrated intensity of the LiF (002) peak. We also observe a weak peak near 90° in χ for LiF (111), indicating that there are some LiF crystals that have their (111) planes parallel with the graphene planes. Figure 4 shows that the peak at $\chi=145^\circ$ increases more rapidly with lithiation than the other regions of the ring corresponding to the randomly oriented crystals. This

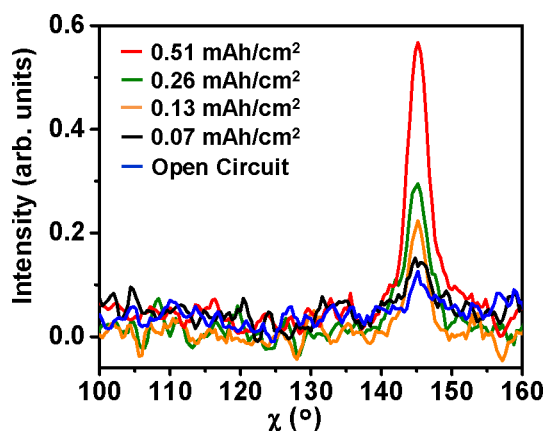


Figure 4. Pole figure, with background subtraction and polarization correction, for LiF (111) at different lithiation stages extracted from MAR CCD images at an incidence angle of 5°.

indicates that the growth of oriented crystals, with (002) planes parallel to the graphene sheets, is favored over randomly oriented crystals after the initial LiF nucleation.

HRTEM was used to further elucidate the morphology of the SEI. Figure 5 shows a representative ex situ HRTEM image of the SEI near the EG/SiC surface after 14 mAh/cm² lithiation, observed along the SiC [2 1̄ 2̄ 0] direction. The SiC (0001) crystal lattice structure is clearly observed in this orientation. The HRTEM image also shows a 0.32 nm spacing of graphene between the SiC crystalline region and SEI. The thick SEI layer contains crystallites whose layer spacing closely matches the (002) d-spacing of LiF. There is also an approximately 3 nm thick region between the graphene and LiF crystals, as well as small regions throughout the rest of the SEI, which appear amorphous. The amorphous-like region at the surface of the EG/SiC indicates that the crystalline LiF is not truly epitaxial with EG/SiC, which is consistent with the X-ray reflectivity. These apparently amorphous regions likely contain randomly oriented LiF and/or other SEI components that were detected with XPS.

CONCLUSION

We find that the SEI formed on the EG/SiC surface is composed of LiF and other common SEI products that are also found on graphite. In situ X-ray scattering shows that LiF formed on the graphene sheets is crystalline, whose amount and vertical domain size increase with lithiation dose. Furthermore, these crystals show texturing, which strengthens

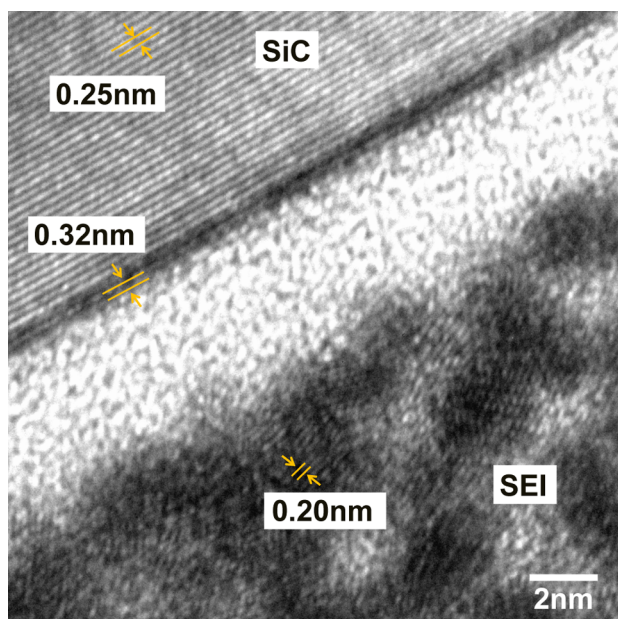


Figure 5. Ex situ HRTEM near the EG/SiC surface taken along the SiC [2 12 0] for a 14 mAh/cm² lithiated EG/SiC sample, showing the structure of the SiC, the graphene layers, and the solid electrolyte interphase (SEI) with LiF crystals.

with lithiation, with their (002) planes aligning close to parallel with the graphene sheets with an orientation distribution width of 2.4° at 0.51 mAh/cm². However, no other diffraction peaks were found, indicating that the other SEI compounds are amorphous. Ex situ HRTEM indicates some apparently amorphous material between the graphene surface and the region with LiF crystallites, thus confirming the conclusion from X-ray reflectivity that the crystalline LiF does not grow directly on the graphene surface. There is also additional amorphous material throughout the SEI that indicates the formation of other SEI components or misoriented LiF. The understanding that LiF forms textured crystals, along with other amorphous SEI components, will allow for more accurate modeling of Li⁺ diffusion and stability of the SEI on graphitic surfaces. These new models will inform ongoing efforts to realize Li-ion batteries with improved rate capability, safety, and lifetime.

■ ASSOCIATED CONTENT

📄 Supporting Information

X-ray thin-film cell design, X-ray scattering geometry, X-ray scattering data at the local specular positions for LiF (111) (Roper CCD) and LiF (002) (MAR CCD), and pole figure construction. This material is available free of charge via the Internet at <http://pubs.acs.org>.

■ AUTHOR INFORMATION

Corresponding Author

*E-mail: bedzyk@northwestern.edu; m-hersam@northwestern.edu.

Author Contributions

[§]These authors contributed equally and are co-first authors.

Notes

The authors declare no competing financial interest.

■ ACKNOWLEDGMENTS

This research was supported by the Center for Electrical Energy Storage, an Energy Frontier Research Center funded by the U.S. Department of Energy, Office of Science, Office of Basic Energy Sciences (Award Number DE-AC02-06CH11357). We also acknowledge the use of Northwestern University and Argonne National Laboratory user facilities including the NUANCE Center, DND-CAT, and NSF-supported MRSEC facilities. We would further like to acknowledge the help of Dr. Jinsong Wu and Benjamin Myers with TEM sample preparation and imaging.

■ REFERENCES

- (1) Peled, E. *J. Electrochem. Soc.* **1979**, *126*, 2047.
- (2) Vetter, J.; Novak, P.; Wagner, M. R.; Veit, C.; Moller, K. C.; Besenhard, J. O.; Winter, M.; Wohlfahrt-Mehrens, M.; Vogler, C.; Hammouche, A. *J. Power Sources* **2005**, *147*, 269.
- (3) Chu, A. C.; Josefowicz, J. Y.; Farrington, G. C. *J. Electrochem. Soc.* **1997**, *144*, 4161.
- (4) Hirasawa, K. A.; Sato, T.; Asahina, H.; Yamaguchi, S.; Mori, S. *J. Electrochem. Soc.* **1997**, *144*, L81.
- (5) Lipson, A. L.; Ginder, R. S.; Hersam, M. C. *Adv. Mater.* **2011**, *23*, 5613.
- (6) Santner, H. J.; Korepp, C.; Winter, M.; Besenhard, J. O.; Moller, K. C. *Anal. Bioanal. Chem.* **2004**, *379*, 266.
- (7) McArthur, M. A.; Trussler, S.; Dahn, J. R. *J. Electrochem. Soc.* **2012**, *159*, A198.
- (8) Bar-Tow, D.; Peled, E.; Burstein, L. *J. Electrochem. Soc.* **1999**, *146*, 824.
- (9) Blyth, R. I. R.; Buqa, H.; Netzer, F. P.; Ramsey, M. G.; Besenhard, J. O.; Golob, P.; Winter, M. *Appl. Surf. Sci.* **2000**, *167*, 99.
- (10) Andersson, A. M.; Edstrom, K. *J. Electrochem. Soc.* **2001**, *148*, A1100.
- (11) *Basic Research Needs for Electrical Energy Storage*; Office of Basic Energy Sciences, Department of Energy: Washington, DC, 2007.
- (12) Lu, M.; Cheng, H.; Yang, Y. *Electrochim. Acta* **2008**, *53*, 3539.
- (13) Peled, E.; Tow, D. B.; Merson, A.; Gladkich, A.; Burstein, L.; Golodnitsky, D. *J. Power Sources* **2001**, *97–8*, 52.
- (14) Peled, E.; Golodnitsky, D.; Ardel, G. *J. Electrochem. Soc.* **1997**, *144*, L208.
- (15) Kanamura, K.; Tamura, H.; Takehara, Z. *J. Electroanal. Chem.* **1992**, *333*, 127.
- (16) Leroy, S.; Martinez, H.; Dedryvère, R.; Lemordant, D.; Gonbeau, D. *Appl. Surf. Sci.* **2007**, *253*, 4895.
- (17) Yan, J.; Xia, B.; Su, Y.; Zhou, X.; Zhang, J.; Zhang, X. *Electrochim. Acta* **2008**, *53*, 7069.
- (18) Yan, J.; Zhang, J.; Su, Y.; Zhang, X.; Xia, B. *Electrochim. Acta* **2010**, *55*, 1785.
- (19) Winter, M.; Novak, P.; Monnier, A. *J. Electrochem. Soc.* **1998**, *145*, 428.
- (20) Placke, T.; Siozios, V.; Schmitz, R.; Lux, S. F.; Bieker, P.; Colle, C.; Meyer, H. W.; Passerini, S.; Winter, M. *J. Power Sources* **2012**, *200*, 83.
- (21) Olivier, J. P.; Winter, M. *J. Power Sources* **2001**, *97–8*, 151.
- (22) Wang, X.-J.; Chen, H.-Y.; Yu, X.; Wu, L.; Nam, K.-W.; Bai, J.; Li, H.; Huang, X.; Yang, X.-Q. *Chem. Commun.* **2011**, *47*, 7170.
- (23) Wang, Z. X.; Wu, C. A.; Liu, L. J.; Wu, F.; Chen, L. Q.; Huang, X. *J. Electrochem. Soc.* **2002**, *149*, A466.
- (24) Nam, K. W.; Wang, X. J.; Yoon, W. S.; Li, H.; Huang, X. J.; Haas, O.; Bai, J. M.; Yang, X. Q. *Electrochem. Commun.* **2009**, *11*, 913.
- (25) Wang, X. J.; Jaye, C.; Nam, K. W.; Zhang, B.; Chen, H. Y.; Bai, J. M.; Li, H.; Huang, X. J.; Fischer, D. A.; Yang, X. Q. *J. Mater. Chem.* **2011**, *21*, 11406.
- (26) Zeng, D. L.; Cabana, J.; Yoon, W. S.; Grey, C. P. *Chem. Mater.* **2010**, *22*, 1209.

- (27) Sharma, N.; Peterson, V. K.; Elcombe, M. M.; Avdeev, M.; Studer, A. J.; Blagojevic, N.; Yusoff, R.; Kamarulzaman, N. *J. Power Sources* **2010**, *195*, 8258.
- (28) Adams, S.; Rao, R. P. *J. Mater. Chem.* **2012**, *22*, 1426.
- (29) Choi, D.; Xiao, J.; Choi, Y. J.; Hardy, J. S.; Vijayakumar, M.; Bhuvaneswari, M. S.; Liu, J.; Xu, W.; Wang, W.; Yang, Z. G.; Graff, G. L.; Zhang, J. G. *Energy Environ. Sci.* **2011**, *4*, 4560.
- (30) Aurbach, D.; Ein-Eli, Y. *J. Electrochem. Soc.* **1995**, *142*, 1746.
- (31) Lipson, A. L.; Chattopadhyay, S.; Karmel, H. J.; Fister, T. T.; Emery, J. D.; Thackeray, M. M.; Fenter, P. A.; Bedzyk, M. J.; Hersam, M. C. *J. Phys. Chem. C* **2012**, submitted.
- (32) Garcia, M. E.; Garofalini, S. H. *J. Electrochem. Soc.* **1999**, *146*, 840.
- (33) Yamada, H.; Suzuki, T. S.; Uchikoshi, T.; Hozumi, M.; Kohama, K.; Sakka, Y. *J. Ceram. Soc. Jpn.* **2011**, *119*, 701.
- (34) Fenter, P. A. *Rev. Mineral Geochem.* **2002**, *49*, 149.
- (35) Fenter, P.; Catalano, J. G.; Park, C.; Zhang, Z. *J. Synchrotron Radiat.* **2006**, *13*, 293.
- (36) Ilavsky, J. *J. Appl. Crystallogr.* **2012**, *45*, 324.
- (37) Baker, J. L.; Jimison, L. H.; Mannsfeld, S.; Volkman, S.; Yin, S.; Subramanian, V.; Salleo, A.; Alivisatos, A. P.; Toney, M. F. *Langmuir* **2010**, *26*, 9146.
- (38) Finch, G. I.; Fordham, S. *Proc. Phys. Soc.* **1936**, *48*, 85.
- (39) International Centre for Diffraction Data Card No. 01-071-3743.
- (40) Sirringhaus, H.; Brown, P. J.; Friend, R. H.; Nielsen, M. M.; Bechgaard, K.; Langeveld-Voss, B. M. W.; Spiering, A. J. H.; Janssen, R. A. J.; Meijer, E. W.; Herwig, P.; de Leeuw, D. M. *Nature* **1999**, *401*, 685.
- (41) Jimison, L. H.; Salleo, A.; Chabinyk, M. L.; Bernstein, D. P.; Toney, M. F. *Phys. Rev. B* **2008**, *78*.
- (42) Belman, N.; Acharya, S.; Kononov, O.; Vorobiev, A.; Israelachvili, J.; Efrima, S.; Golan, Y. *Nano Lett.* **2008**, *8*, 3858.